Universiteit Utrecht

Bachelor's programme Physics and Astronomy

The heating of Molybdenum diselenide An in-situ Transmission Electron Microscopy and Density Functional Theory study

Bachelor Thesis

S.C. van Aartsen

Supervisors:

Dr. ir. M.A. van Huis

Debye Institute for Nanomaterials Science

D.S. Gavhane MSc

Debye Institute for Nanomaterials Science

June 12, 2019

Abstract

In recent years nanomaterials have aroused a lot of interest among researchers. Nanomaterials have a wide spectrum of applications ranging from electronics to catalysis. However, much is still unknown about these nanomaterials: what material or composite material is the best for which application and how to modify the properties of these materials in the desired way. This study contributes to the fundamental knowledge of the two-dimensional nanomaterial molybdenum diselenide, $MoSe_2$. We investigate the thermostability of this material by in-situ transmission electron microscopy. This technique allows to do real-time, atomic scale imaging while heating up to over a thousand degrees Celsius. At this high temperatures, starting from around 850 °C the material decomposed by the selenium sublimation into the vacuum of the elctron microscope. At slightly more moderate temperatures (750 °C - 850 °C) only a significant amount of selenium sublimates when irradiated by the electron beam. This moderate etching caused spontaneous formation of nanowire networks. The nanowires can be connected to either pristine $MoSe_2$ or elemental molybdenum. Density Functional Theory calculations are used to assist the interpretation of the results. Based on these calculations, many phases are concluded to be energetically unstable, except for two two-dimensional phases (the H-phase and the T-phase) and the observed Mo_6Se_6 nanowire.

Contents

1 Introduction

Transmission Electron Microscopy (TEM) is a powerful tool in material science. It allows to investigate structures up to atomic resolution. The effects that occur due to the nature of the electron beam, like imaging effects at the edges of examined samples, can also be used to gain insights. Furthermore, beam effects also play an important role in electron microscopy: the beam can be destructive to the sample. Of course it is not directly necessary to call it a destructive technique since the imaging damage can be kept small when applying only a small electron dose or low voltage.

On the other hand, the ability to change the structure by high voltage electrons also paves the way to other applications of the electron microscope than only imaging. When carried out in a controlled manner, structures in the sample can be altered at atomic scale while imaging, which is a powerful tool.

Using the electron beam to modify the sample is an example of in-situ electron microscopy: doing experiments *inside* the microscope. However, using the electron beam is only one of the many techniques one can use in-situ. Another important in-situ technique is heating. The sample can be heated up to a few hundred or a thousand degrees Celsius while imaging. This opens the way to investigating changes in the sample that might occur upon heating while it happens, instead of only being able to image after the heating experiment. Besides heating, also other in-situ experiments can be done like applying an electrical current or keeping the particles inside a liquid or gas cell (typically all electron microscopy imaging is done in vacuum).

Here, electron microscopy in-situ heating is used for the material $MoSe_2$. To support the experimental in-situ electron microscopy, Density Functional Theory (DFT) simulations are used. It is commonly used to determine the structure, associated energy and electronic structure of a compound. Furthermore, magnetic properties of the material can be predicted. In the calculations discussed here, the DFT code VASP (Vienna Ab-initio Simulation Package) is used. Other programs can be used as well, as they are all based on the same principles.

Of course, eventually $MoSe_2$ will decompose at a sufficiently high temperature. Thus, determining this decomposition temperature is not the objective of this study. What is interesting to know is what happens before decomposition, finding out whether the structure remains the same or changes. DFT is used to create an overview of possible phases of $MoSe_2$. The energetic favorability of the phases help to declare the phases found in experiment. Normally $MoSe_2$ is found in the H-phase. One question is whether the slightly higher energy T-phase is formed at elevated temperatures. However also other structures might form, which has to be found out. And in case of (partial) decomposition or etching, the question is in what manner this happens. The same question arises for defects in the crystal structure. In all cases mentioned here, the role of the electron beam is important. The distinction between areas imaged under electron beam irradiation and areas that are not should be explicitly made since it already is shown extensively that the beam can have a huge effect on structures found in the imaged imaged.

$MoSe_2$ is a semiconductor and therefore has possible applications in electronics or catalysis. Knowing what happens upon heating contributes to the fundamental knowledge of this material, eventually leading to applications. Consider the T-phase, which is conducting in contrast to the H-phase which is semi-conducting. When these or other distinct phases form upon heating, knowledge gained in this study substantially contributes to the ability to control the formation of these phases. The same holds for the the behaviour of edges and defects when exposed to

high temperatures. The possibilities of high temperatures, with or without the assist of electron beam irradiation, being a proper instrument to modify this material is explored.

2 Theoretical background

2.1 Two-dimensional materials

$MoSe_2$ is a two-dimensional material: it consists of layers stacked together. The most well-known 2D material undoubtedly is graphene. However, graphene is not the only 2D material with interesting (electronic) properties. Transition metal oxides (TMOs) and transition metal dichalcogenides (TMDs) are two classes of materials that have aroused much interest among researchers. A typical semiconductor TMD is MX_2 with M = Mo or W and X = S, Se or Te. Of these, MoS_2 is studied most because of its stability.[1] Moreover, in many cases, properties of the bulk differ from those of the 2D material, the latter having only a few or even only one layer. For example, some TMDs, like $MoSe_2$, go from an indirect bandgap in the bulk to a direct one when exfoliated.[2] This is an interesting feature to investigate because many TMOs and TMDs are semiconducting with appropriate bandgaps (1-2 eV) for optoelectronics.[2] This means that if we fully understand and are able to tune the electronic properties of the material, by making large doped 2D layers or multi-layered stacks for example, the applications in the semiconductor or catalyst industry can be vast.

2.1.1 Synthesis

Typically, TMDs can be found in bulk materials where sheets of the 2D-material are randomly stacked together. Different techniques can be used to separate these layers. An easy method to separate layers and obtaining the monolayers of high purity is using adhesive tape, which is a form of mechanical cleavage of the layers.[2] A drawback is that the 2D material cannot be obtained in large quantities and that size and thickness can hardly be controlled.[2] One has to try and hope to extract a single layer, when desired.

Another method widely used for separating layers is liquid phase exfoliation (LPE). Bulk material is brought in a solvent, the solvent molecules are able to intercalate between the layers, which result in exfoliation. Probe sonication is often used to enhance this process.[3] Jawaid et al.[3] investigated the mechanism behind the intercalation, with MoS_2 as model for other TMDs. They found that *N*-methyl-2-pyrrolidone (NMP) is the most effective solvent. Their technique is solvent-assisted and thus additive free, in contradiction to Joensen[4] and co-workers who were the first to separate thin layers TMD material. They used a lithium additive compound to form H_2 gas bubbles that separate the layers.

A last method to produce 2D-materials (or TMDs especially), that will not be discussed in detail here, is chemical vapour deposition (CVD). In this method, a vapour is condensed on a substrate to form the material bottom-up.[2] CVD is promising to obtain large flakes with high purity in large amounts. Also, it can yield monolayer material, in contrast to using LPE on bulk material where obtaining monolayer might be hard to achieve. Monolayer $MoSe_2$ can be synthesised by reacting MoO_3 and Se at 750 °C on a Si wafer with silica top layer.[5] The reactants are carried by a gas flow consisting of argon with 15% hydrogen.

2.1.2 Applications

As stated before, the properties of 2D materials can differ from those of the bulk material. This opens the door to many applications of this kind of nanomaterial. One of the interesting properties of 2D TMDs is that they are semiconducting. Even better, this semiconduction can be tuned by altering the structure of the material as shown for among others MoS_2.[6] Applications in the semiconductor industry are still immature, however seem promising. In many articles, the possible applications are emphasized. The electronic properties can be tuned in a variaty of ways; defects, doping, edges, nanowires, grain boundaries, etcetera. Already some nano-electronic components have been shown to be possible on MoS_2.[7]

2.2 Structure of TMDs

A single layer is quite similar for different kinds of TMDs, most of them have the same structure. This structure consists of three atomic layers. The top and bottom layer are formed by hexagonal structures of the chalcogen atoms, the middle layer consists of the transition metal atoms. $MoSe_2$ has this structure. In its most common form, the molybdenum atoms have a trigonal prismatic coordination, called the H-phase. In the T-phase, the molybdenum has an octahedral coordination. Both phases imply that each is bound to six selenium atoms, and each selenium atom to three molybdenum atoms.[2] In bulk material, the sheets are held together by Van der Waals forces.[3] Upon exfoliation, the phase might change. For MoS_2 it was found to change to 1T for monolayer.[8]
Layers can be stacked upon each other in a variety of orientations, in which monolayers are translated differently, like 3R (layers with three altenating translations). In bi-, tri- or few layered $MoSe_2$, oriented stacking is observed for most regions. Both 2H and 3R stacking occur for naturally occuring $MoSe_2$.[9] The number in front indicates the number of layers in one repetition. Monolayer H-phase for example is indicated as 1H.

2.2.1 Defects

It is known that vacancies and other defects in graphene influence many of the properties of the material. However, the effects of defects in TMDs have barely been studied.[10]

Zhou et al.[10] systematically studied defects in MoS_2 using Annular Dark Field Scanning Transmission Electron Microscopy (ADF-STEM). They identified six different point defects: monosulfur vacancy, disulfur vacancy, a vacancy of molybdenum and three neighbouring sulfur atoms, a vacancy of a Mo-atom and six neighbouring sulfur atoms, a Mo-atom replaced by two sulfur atoms and two sulfur atoms replaced by one Mo-atom. Of these effects, the formation energy was calculated by density functional theory. It turned out, single Mo-atom vacancies were not observed alone, because the binding energy of the surrounding S-atoms decreases dramatically upon removing the Mo-atom. Since the electron beam energy was lower than the knock-on threshold, presumably the vacancies are caused by beam-induced ionisation or via contamination.[10] Furthermore, the vacancies can, under the right conditions be filled with other elements to do electron-beam-induced doping.[11]
It can be expected that $MoSe_2$ exhibits similar point defects as MoS_2. An elaborate study on point defects in $MoSe_2$ has not been done, but of course point defects have been observed in $MoSe_2$ using ADF-STEM.[9]

Just as there is a variety of vacancies (point defects), there also is a variety of line defects and grain boundaries (GBs) in 2D materials. These GBs can be seen in high resolution TEM (HR-TEM) but also DFT-calculations are popular to predict different kind of boundaries, their stability and formation energy. In graphene, these dislocations and GBs have been studied extensively[12]. In graphene, all GBs consist of pentagon-heptagon pairs (indicated 5|7). This is because the formation energy of the boundary is only determined by the strain of the rings, which is lower for 5|7 than for 4|8 for example.[12] Liu et al.[12] described GBs in 2D boron nitride (h-BN) and found 4|8 is the most favourable boundary. Any strain can be relaxed in the z-direction Because this is a multi-element structure, also the energy difference between homo- and hetero-elemental bonding plays a role. In the calculations the energy is calculated by subtracting the total energy of the pristine lattice from the energy of the altered one.[7] The dislocations are introduced by removing some atoms from the lattice and reconnect the sides of the introduced cut. This alteration is described by the Burgers vector.[7] GBs can be described as a series of dislocations.

TMDs show similar dislocations, however the z-direction is a more important factor because of the three atomic layers, as Zou et al.[7] showed for MS_2 (M = Mo, W). Here 4|8 was found unstable, 5|7, 6|8 or 4|6 were found more stable, depending on the conditions (M- or S-rich environment). Using DFT they were able to calculate the energy as function of the tilt angle between the two regions separated by the GB.

In monolayer $MoSe_2$ line defects are shown to be similar to those in MoS_2. For example 21° (5|7) and 60° (4|4P) GBs are found both in $MoSe_2$ and MoS_2.[9] The 'P' in the latter indicates that the two 4-fold rings are point-sharing. The 60° boundaries are also called mirror-twin-boundaries (MTBs). Lehtinen et al.[13] studied this kind of GBs in $MoSe_2$, both right after synthesis by CVD and electron beam induced GB formation. For the CVD synthesized sample, they reasoned that the MTBs are formed during the growth of an individual grain, not by the merge of two grain. The quantity of GBs could be tuned by using Mo-rich or Se-rich conditions. More Se-deficit MTBs were formed in Mo-rich conditions. To wit, the by Lethinen et al. observed MTBs have a surplus of $1.00\,\mathrm{nm}^{-1}$ Mo atoms. Control on GBs during growth is not really possible, however it is controllable using beam induced boundary formation. Lehtinen et al. did DFT calculations on the MTBs. They found that MTBs are favoured over many Se-vacancies in $MoSe_2$.

GBs have electronic properties different from the pristine 2D material. For example, calculations show that the 60° GB is metallic, in contrast to semi-conducting pristine $MoSe_2$ or MoS_2.[9] Using this, a complex electronic structure can be given to the 2D material. Also control over edges of flakes is important to tune the electronic properties.[14]

2.3 Transmission Electron Microscopy (In-situ)

The studies stated in the above sections mainly used, besides the ones that are based on calculations, TEM or STEM to analyse the material. (S)TEM offers the ability to study materials up to atomic scale. However, normally this isn't a real-time investigation, experiments on the sample are executed before it is imaged in the electron microscope. With in-situ TEM, one is able to study the material *while* exposed to external stimuli.[1] These stimuli can be various, including controlled electron beam irradiation, heating, applying an electrical current and applying mechanical stress. The first two are looked into in more detail here. On top of that, these conditions can be combined with in-situ CVD.[15] Then, formation mechanism can be studied in detail, possibly assisted by electron beam irradiation or heating.

2.3.1 Electron beam irradiation

Electron beam damage (knock-on or ionisation) can be a negative side effect of the electron beam and is worst for polymers or organic substances but also inorganic materials are affected by the beam.[16] However, the beam can also be used as tool to alter the sample in quite a precise way. One application is be the making of nanopores in the 2D-material.[1] Hereto, the transferred beam energy should be close to the bonding energy of the atoms, to construct the hole in a controllable way. Whenever there is a small hole, atoms at the edge will be knocked off more easily[17], which matches the findings on vacancies described in section 2.2.1. Thus, larger holes can be made quite easy.

As Liu et al.[17] show, this also paves the way for in-situ constructing of nanowires (NWs). They found that when two holes meet, the material in between is narrowed and instead of breaking, a NW with a width of 0.35 nm forms. Later, Lin et al.[18] also fabricated NWs, up to 10 nm length, for other TMDs ($MoSe_2$, WSe_2 and again MoS_2), as was expected to be possible as well. For all three, Lin et al. found a 1:1 ratio of the elements in the NW, DFT calculations predicted this structure to be the most stable. The NWs are even more stable than the edge of the pristine material (higher sulphur vacancy formation energy).[17] This explains why the wires are self-healing: when a S- or Se-atom is removed by the electron beam, it is quickly replaced by diffusion.[18] Furthermore, it is was also possible to fabricate junctions and it was shown that the wires are metallic.

This, however, was not the first time TMD nanowires were observed. In 1985, long fibers (up to 10 µm) of the anorganic polymer MoSe were observed.[19] The production of the fibers was totally different: $Li_2Mo_6Se_6$ was dissolved, upon which bunches of fibers were observed (up to 20 Å thin). Later, also single fibers were observed with the same structure as the one made in-situ.[20]

2.3.2 Heating experiments

With in-situ heating, it is possible to maintain atomic resolution up to 1200 °C.[1] At higher temperature, the thermal drift caused by expansion is the main reason of the loss of resolution.

Often, the objective of TEM in-situ heating experiments is an analysis on thermostability or a controlled synthesis.[1] An example of a heating experiment on TMDs is an experiment by Zink et al.[21] They synthesised amorphous spherical WS_2 and MoS_2 particles by metal-organic CVD, upon which the temperature was raised. The most important change that was observed for both species was the crystallisation with increasing temperature. However, even at low temperatures (250 °C), crystalline areas could be seen. The crystalline lattices have the tendency to align with the edge of the sphere, lowering the energy. Eventually, the spheres became hollow. Another effect of the heating was the healing of defects. This can be an interesting application of heating TMDs, because defects can have a negative effect on possible electronic applications. Interestingly, irregular shaped particles did not become hollow, the healing of defects was the only change observed.

Another example of in situ heating is the study of Sang et al.[14] into edge evolution upon heating of W-substituted $MoSe_2$ ($Mo_{0.95}W_{0.05}Se_2$). The CVD-synthesized sample was heated rapidly to 500 °C. Four kinds of edges were found stable, of which the most simple is a Mo-zigzag edge (comparable to a zigzag edge in graphene) terminated with Se. Se-zigzag edges were only found

stable with a GB with a Mo-zigzag terminated with Se. The other two stable edges were Mo_6Se_6 nanowire-like edges, with the same structure of the NWs as discussed in section 2.3.1.

The edge structure has influence on the etching rate. NW-like edges prefer to etch in a direction parallel to the edge, Se-terminated edges along the lateral direction. Sang et al. observed that a hole consisting of NW-like edges grows towards a triangular hole, because zigzag-Mo-NW edges etch faster than zigzag-Se-NW edges. These observations were supported by DFT-calculations. However, carbon residue from CVD-synthesis influences edge formation. In areas with heavy carbon residue, edges were not as straight as in areas with lower residue.

A final example, which is interesting for the experiment described here, is the phase transition from the H-phase to the T-phase of MoS_2 upon in-situ heating.[6] Lin et al. heated Re-doped MoS_2 (<1 at%) up to a few hundred degrees Celsius. The phase transition could clearly be seen from the TEM image. The transition occurred via an intermediate state (α-phase) in which zigzag-Mo rows lie closer to each other than in pristine 2H MoS_2. When two α-phases with meet with an angle of 60°, the strain makes S-atoms shift towards the T-phase. The resulting triangle with this phase can further expand. The Re-doping is thought to be beneficial for easing the α-phase formation. Furthermore, the electron beam irradiation plays an important role here. Below a certain electron dose threshold, the phase transition does not occur, independent of temperature. The dependence on radiation opens the door to selective irradiation if the beam can be focused precise sufficiently. Since the H-phase is semiconducting and T-phase is metallic, electronic structures might be produced using electron irradiation. Lin et al. already showed immature prototypes like a junction that could be used as transistor.

When doing in-situ thermostability experiments, it is important to have a reference of the ex-situ experiment. Already in 1969, NASA has done experiments on the thermal stability of TMDs.[22] $MoSe_2$ and other TMDs were heated after which the mass loss was measured. For $MoSe_2$ detectable mass loss started around 800 °C. In general, it was found that the selenides lost weight at somewhat lower temperatures that the equivalent sulfides. Furthermore, the materials were suspected to dissociate at lower temperatures, but this could not be detected. A fluorescence measurement showed that all selenium had been gone above 1200 °C.

2.4 Principals of Density Functional Theory

The principle upon which DFT is based were first described by Hohenberg and Kohn[23]. They showed that a given potential is determined by a unique charge density. They also concluded that there exists an energy functional which expresses the energy of the system as function of the electron density, and they proved that minimizing this functional gives the electron density of the ground state.

However for computational feasibility, wavefunctions are introduced. This calculation is done in a few steps listed below[24].

- Initial guess of charge density $\rho(\vec{r})$ based on ion positions.
- Calculation of the effective potential

$$V_{eff}(\vec{r}) = V_{ext}(\vec{r}) + \frac{e^2}{4\pi\epsilon_0}\int \frac{\rho(\vec{r}')}{|\vec{r}-\vec{r}'|}d\vec{r}' + V_{xc}(\rho(\vec{r}))$$

  This potential consists of known terms (potential by the lattice ions and Coulomb inter-

action between the electrons) and the still unknown exchange-correlation potential V_{xc}, which is defined by[25]

$$E_{xc}(\rho) = \int V_{xc}(\rho(\vec{r}))\rho(\vec{r})d^3\vec{r}$$

This exchange-correlation functional is part of the energy functional and it is quite a challenge to find a proper one. In over fifty years, many functionals have been tried, but it is hard to find one suitable for all systems.[25] In this report, only the functionals used for this study will me mentioned.

- Using the effective potential in the Hamiltonian to solve the Kohn-Sham equations (wave equations).
- With the resulting wavefunctions, the electron density is calculated.
- If this calculated density is consistent with the initial guess, the system has been electronically converged. Otherwise the procedure is repeated with the newly found density as guess in step 1.

Whenever the calculations including the wavefunctions are electronically converged, forces on the ions present in the system can be calculated, which is simply the derivative of the energy landscape. Ion positions can be altered in order to obtain a structure with lower energy, the ionic relaxation. Note that this ionic step is completely classical, whereas the electronic steps are quantum mechanical. After each ionic relaxation step, the electronic calculation has to be converged self-consistently again.

For crystals there is a periodic structure, also in reciprocal space. VASP then only has to do calculations in the unit cell of the crystal. The unit cell in reciprocal space is called the first Brillouin zone. For two-dimensional materials, like $MoSe_2$, there is only periodicity in two dimensions. This problem is solved by also introducing periodicity in the z-direction, however with a large cell parameter in this direction. This way, atoms of the different layers are so far away that they do not interact. Of course, if one wants to simulate the bulk phase of a two-dimensional material, this empty space must be made smaller. Important then is to include a Van der Waals-term in the energy functional.

As a final remark on DFT, it is important to note that the described static DFT calculation can only calculate energies and other properties at 0 K. Therefore it is not possible to directly state that a structure with low energy in DFT is the most favourable at elevated temperature. Conclusions can only be drawn if thoroughly supported by high-resolution TEM images and/or other techniques like Energy-dispersive X-ray crystallograpphy (EDX). DFT must be seen as a supplement to these techniques mention. However, conclusions from DFT make more sense if applied to the sample cooled down to room temperature after heating.

3 Methods

The material $MoSe_2$ is not synthesised by ourselves but bought commercially in bulk form. As mentioned, $MoSe_2$ consists of two-dimensional sheets held together by Van der Waals forces. For imaging in the electron microscope, it is important that the sheets are exfoliated as much as possible, preferably only one layer thick. Putting bulk material in the microscope would result in many layers on top of each other which moreover are not aligned. When the sample is

thick, nothing can be seen as the electron beam cannot penetrate in that case. On top of that, misalignment of layers result in difficulty in determining the structure.

For the analysis of the experimental results, DFT calculations are used. Multiple phases are modelled, of which most importantly the internal energy can be determined.

3.1 Liquid Phase Exfoliation

To separate the layers of $MoSe_2$, liquid phase exfoliation (LPE) is used. Hereto, 44.2 mg $MoSe_2$ is dissolved in 50 mL ethanol (for some experiments isopropylalcohol is used) and then diluted with a factor 10. Since the layers are not directly exfoliated upon dissolving, probe sonication is used to enhance the LPE process. The solution is probe sonicated with a 40 kHz probe sonicator for a few hours. Since much energy is added to the solution, one must be careful that the solutions does not get too hot. Therefore the pulse mode is used: the sonication is switched on and off (10 seconds on, 3 seconds off) alternatingly. The peak power of the probe sonicator is 40 W. However, still a visible amount of solvent is evaporated during probe sonication. The concentration of $MoSe_2$ thus changed, however for the experiment this is of low importance. To prevent flakes from attaching again, just before use for each experiment, the solution is sonicated under the same conditions for only 5 minutes. To image the $MoSe_2$ in the microscope, a droplet of the solution is dropcasted on a grid upon which the solvent evaporates and the $MoSe_2$ remains.

3.2 In-situ heating

The sample was imaged mostly with a FEI Talos F200X electron microscope, with an electron acceleration voltage op 200 kV. Some experiments were done on a FEI Titan electron microscope, with a voltage of 300 kV. For the in-situ heating, special DENSsolutions heating holders are used, to heat the sample from room temperature up to a maximum of around 1000 °C. Going upwards in temperature is done in steps of at most 50 °C. This way it is assured that the Si_3N_4 support membranes will not break upon a sudden temperature rise and furthermore it is possible to keep track of changes in the sample while heating.

Most images were made in TEM Bright Field mode, because most of the times this gave a better resolution than High Angle Annular Dark Field (HAADF) STEM mode. The resolution can be seen directly from the screen but also the Fast Fourier Transform (FFT) image can help. When more dots in a hexagonal pattern are visible in the FFT, the resolution is better. Moreover, the FFT also helps to quickly determine whether there is a single orientation or multiple: multiple hexagonal patterns in the FFT image indicate multiple orientations. However, layers with different orientations on top of each other are also quickly spotted on the screen by the Moiré patterns they produce. (figure 1) FFT is also useful afterwards for the analysis of the images: the spots of the hexagonal pattern can be filtered out. After applying the reverse Fourier transform, an enhanced image is obtained in which the structure of the material is better visible.

The resolution can be cranked up by imaging a flake above a hole in the supporting material. The $MoSe_2$ is supported by silicon nitride (Si_3N_4). Si_3N_4 is amorphous and is not visible clearly (in the FFT as vague rings) because it is thin. However when due to the high intensity electron beam a hole has formed in the Si_3N_4 and a part of the flake is above this hole, the atomic

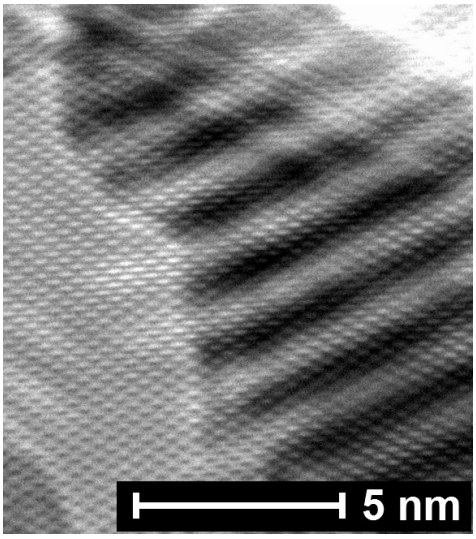

Figure 1: TEM image of a Moiré pattern in multilayer $MoSe_2$. This indicates the layers are not aligned.

resolution is really clear (figure **??**). When a hole has been formed in the Si_3N_4, it is important to be careful with the strong electron beam, to prevent the hole from growing too large and loosing the flake of $MoSe_2$. When imaging with atomic resolution, a magnification of around 10^6 is needed, for which (at the FEI Talos electron microscope) a beam intensity of 10^6 e/nm^2/s up to 10^7 e/nm^2/s is needed to obtain a sufficiently bright image. This is a high dose, which will definitely expand the hole if there is one.

3.3 Energy-dispersive X-ray spectroscopy

In STEM mode, the electron microscope offers a powerful tool to determine which atoms are in the sample: Energy-dispersive X-ray spectroscopy (EDX). An EDX detector in the electron microscope measures X-rays emitted by the atoms in the sample upon irradiating with the electron beam. Since every atom has its own characteristic emitted X-ray wavelengths, it is possible to create a quantitative image of the atoms present. For $MoSe_2$ a Mo:Se ratio of 1:2 is expected at room temperature before intensively irradiating in the electron microscope. However, more EDX measurements are done also after irradiation and heating. Due to limitations of the equipment it is only possible to measure the EDX spectrum after cooling down and not during heating.

3.4 Atomic Force Microscopy

When combined with other techniques, it is possible to gain a more complete view of the material investigated. Here, besides in-situ heating of $MoSe_2$, Atomic Force Microscopy (AFM) is used. This technique provides a height map of a sample, which is suitable for a layered two-dimensional material. Here, AFM can provide information on the manner $MoSe_2$ is layered. Knowing this, it

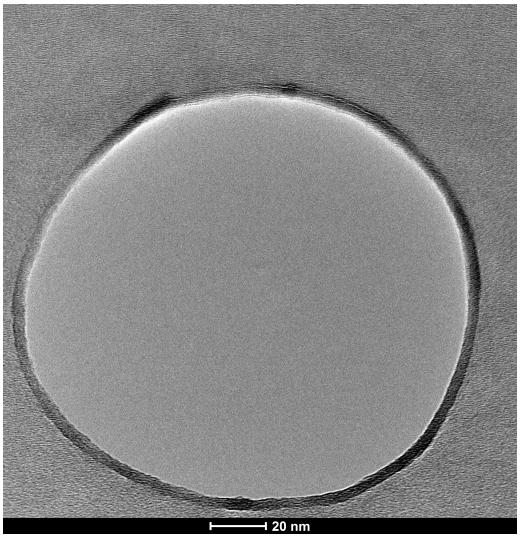

Figure 2: TEM image of a hole in the Si_3N_4 background. When a $MoSe_2$ flake 'hangs 'over the edge, better resolution can be achieved.

is more easy to interpret images from the electron microscope. From the same solution of $MoSe_2$ a sample was dropcasted on a mica sheet and imaged with AFM. Unfortunately, the heating chips used for in-situ TEM are not suitable to use for AFM. Therefore, only $MoSe_2$ from the stock solution is measured using AFM and not after in-situ heating.

3.5 Density Functional Theory calculations

Different phases of $MoSe_2$, and other phases with an other ratio between Mo and Se atoms, are examined using VASP[26][27][28][29]. PAW-potentials[30][31] are used for the atom potentials. As exchange-correlation functional the PBE-method is used.[32] Because some of the phases examined consist of monolayers, Van der Waals interactions might be quite important, therefore a correction on the functional is added: the DFT-D3 correction method with Becke-Johnson damping.[33][34] First, the structure is ionically relaxed by setting the NSW-tag to a value higher than 0, which means ionic steps are done. Later, in a following calculation, information about the phase is obtained, like the band structure, the density of states (DOS), and magnetic moments. There is an important difference in calculating the first two. The band structure is calculated along high-symmetry lines in the first Brillouin zone. Hereto, a path of k-points in the first Brillouin zone must be defined by hand. The k-points define which points in the first Brillouin zone VASP uses for the calculation. In a hexagonal structure commonly a triangular shaped path is defined: from the central Γ-point via the K- and M-point back to the Γ-point. On the other hand, the DOS is calculated with an automatically generated evenly distributed k-mesh. This is the same k-mesh as used in the ionic relaxation calculations. For a two-dimensional material, the height of the unit cell in the z-direction is large, which means a small first Brillouin zone in the reciprocal z-direction. A suitable k-mesh (x*y*z) was found to be (16*16*1) or (16*16*2). This is based on energy fluctuations between different mesh sizes. Large meshes ensure low fluctuations, which should be below 0.5 meV/atom, but too large meshes have a long calculation time. 1T-phase $MoSe_2$ was used to determine the optimal size of the k-mesh (figure

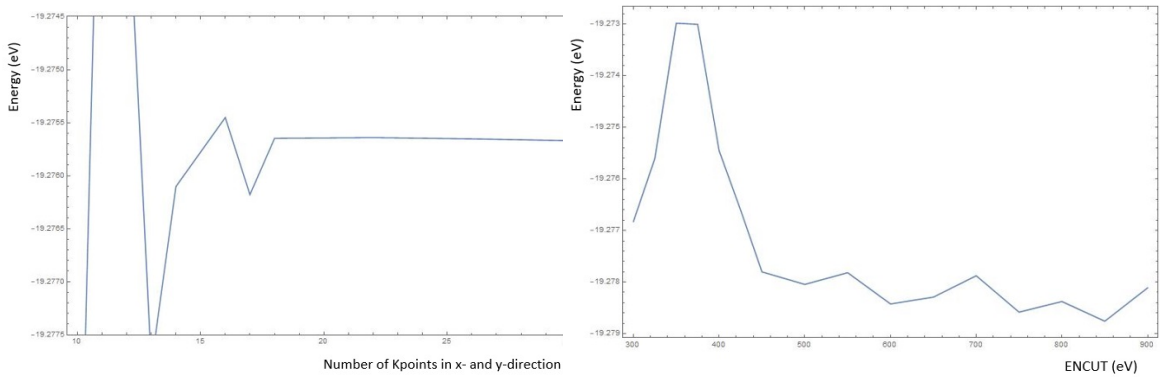

(a) (b)

Figure 3: Fluctuations in energy of 1T-phase $MoSe_2$. (a) The k-points on the horizontal axis determine the number of k-points used in x- and y-direction of reciprocal space (k*k*1). For k=16, the energy fluctuation are below 0.5 meV/atom. (b) ENCUT-variation for the $MoSe_2$ 1T-phase. For ENCUT=600, the fluctuations are below 0.5 meV/atom.

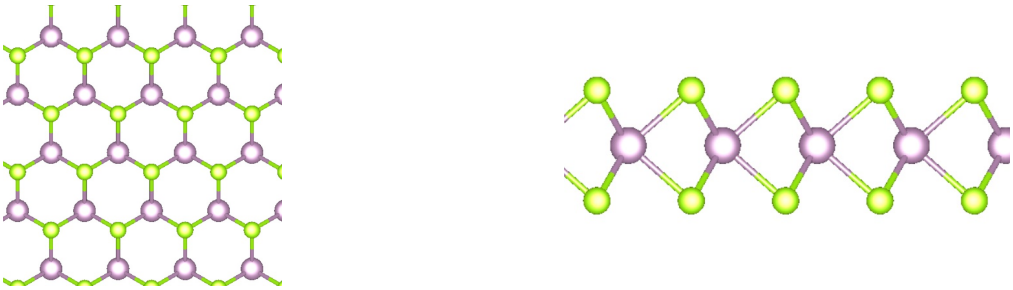

Figure 4: Atomic model of 1H phase $MoSe_2$. All atomic models in this thesis are made with VESTA software.[35]

3a). The same must be done for another parameter in VASP: the ENCUT- and ENAUG-tag (figure 3b). These tags set the cutoff energy for the plane waves used in the calculation. It was found that ENCUT = 600 eV is suitable with, by default, ENAUG = 1.4 x ENCUT = 840 eV.

3.5.1 $MoSe_2$

For monolayer $MoSe_2$, there are two main structures: the 1H and the 1T phase (figure 4 and 5). Both are known from literature as discussed in section 2.2.

From these two structures the internal energy is calculated, and also the density of states (DOS) and band structure. These data of these structures are already known from literature[36], the calculations here serve as confirmation. The formation energy is calculated by equation 1. Equation 1 is the general form of the formation energy, for $MoSe_2$ x = 1 and y = 2. The formation energy thus is the energy with reference to the elements it contains, which implies elements always have formation energy 0 by definition. The molybdenum taken as reference here is in BCC

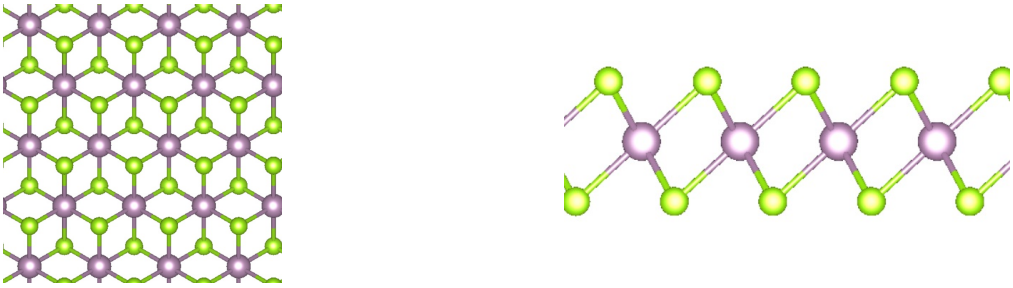

Figure 5: Atomic model of 1T phase $MoSe_2$

(a) (b)

Figure 6: Atomic model of H-type MoSe **(a)** Top view **(b)** Side view

phase and the selenium has a hexagonal structure (gray selenium).

$$E^f = E_{Mo_xSe_y} - xE_{Mo_2} - y\frac{1}{3}E_{Se_3} \tag{1}$$

3.5.2 MoSe

Now, different phases of MoSe are examined. It is interesting to do DFT calculations on MoSe structures (Mo:Se ratio of generally 1:1) because in heating experiments, it is possible that the Mo:Se ratio changes and therefore new phases might form. As with the two $MoSe_2$ phases, the structures are relaxed and then some properties (formation energy, DOS and magnetization) are calculated. The following phases are examined:

- MoSe H-bulk phase (figure 6)
- MoSe T-bulk phase (figure 7)
- Flat hexagonal MoSe (figure 8)
- Wavy hexagonal MoSe (figure 9)
- Flat square MoSe (figure 10)

Of course more structures are possible, the number of possible phases is infinitely large if all Mo:Se ratios are allowed. Here, however, we stick to some simple ones which could possibly have an energy sufficiently low to occur.

(a) (b)

Figure 7: Atomic model of T-type MoSe **(a)** Top view **(b)** Side view

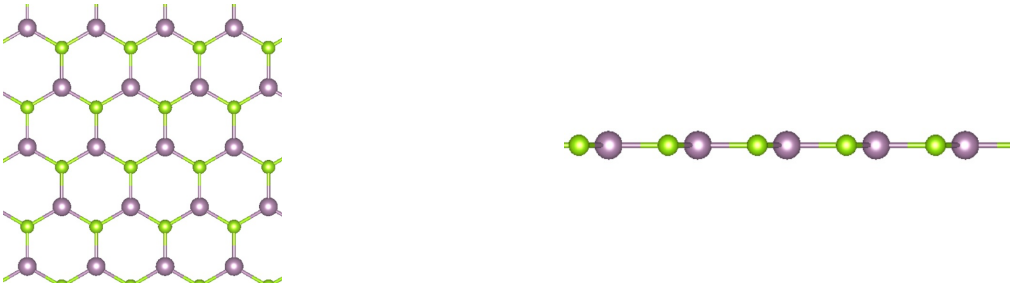

Figure 8: Atomic model of flat, hexagonal MoSe

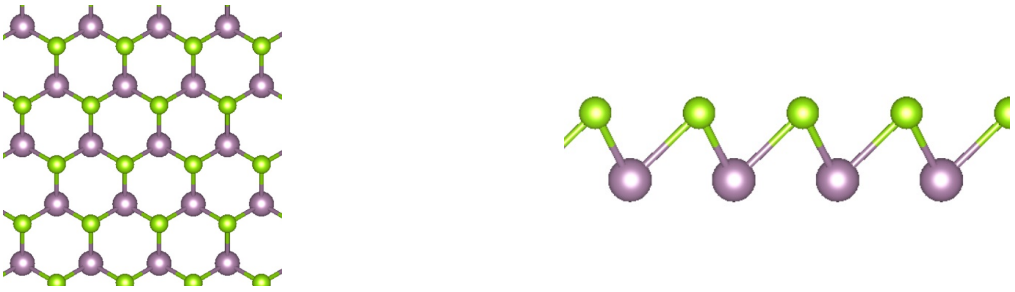

Figure 9: Atomic model of hexagonal MoSe

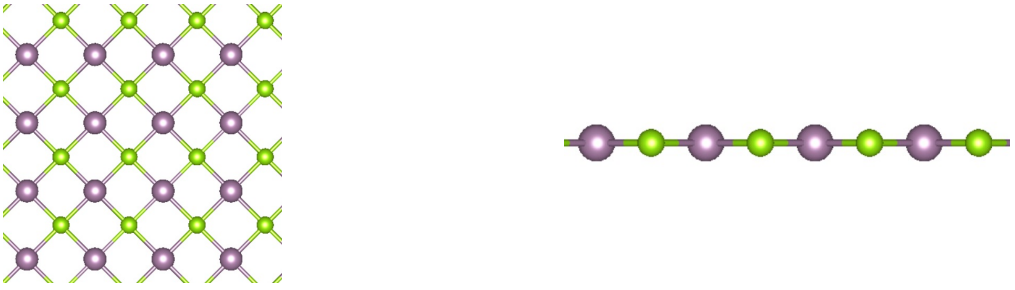

Figure 10: Atomic model of MoSe with a square lattice

Table 1: Nanowires calculated with DFT

Nanowire	Remark
Mo_4Se_4 (figure 11)	Inspired by structure below
Mo_6Se_6 (figure 12)	Found most favourable by refs [37] and [18]
Mo_8Se_8 (figure 13)	Inspired by structure above
$Mo_{10}Se_{10}$ (figure 14)	Inspired by structure above
Mo_5Se_4 (figure 15)	Suggested by ref [17]

Figure 11: Atomic model of Mo_4Se_4 nanowire

3.5.3 Nanowires

With Mo and Se atoms, small nanowires can be constructed. For $MoSe_2$ and materials similar to $MoSe_2$ like MoS_2, nanowires have been observed clearly and also their structure have been determined using DFT, among others by Lin et al.[18] as discussed in section 2.3.1. For all materials they investigated, Lin et al. found a nanowire structure with Mo:Se ratio of 1:1. From now on, this ribbon is refered to as the Mo_6Se_6 nanowire since both atoms are present in the unit cell six times. The other nanowires investigated here are named in a similar manner. Different nanowire structures are compared, following earlier comparisons[37][17]. Table 1 summarizes all ribbons that is considered by DFT.

Note that the first four have a comparable structure. It is checked which of those four has the lowest energy and what the reason is for that. For the most stable nanowire of the five above, additional properties like the DOS, band structure and magnetism is calculated.

Figure 12: Atomic model of Mo_6Se_6 nanowire

Figure 13: Atomic model of Mo_8Se_8 nanowire

Figure 14: Atomic model of $Mo_{10}Se_{10}$ nanowire

Figure 15: Atomic model of $Mo_{54}Se_{54}$ nanowire

3.5.4 Threshold Displacement Energy

When investigating materials in the electron microscope, in general one wants to minimize effects by the microscope itself i.e. electron beam effects. On the other hand, in some cases the beam effects can be used to change the structure in a more or less controlled way, as discussed as one of the forms of in-situ electron microscopy in section 2.3.1. In both cases it is useful to know how susceptible the material is to the energy of incoming electrons. DFT can be used to calculate the amount of energy $E^f_{vac,Se}$ needed to remove a Se-atom from the structure, also called the vacancy formation energy:

$$E^f_{vac,Se} = E_{Mo_xSe_{y-1}} + \frac{1}{3}E_{Se_3} - E_{Mo_xSe_y} \tag{2}$$

Here, the term elemental selenium is added to equate the number of atoms in the equation. Since VASP works with periodic lattices, a removal Se-atom is also periodic, and only using the lattice unit cell is not sufficient. A larger supercell is defined in which one atom is removed. Here $E^f_{vac,Se}$ is calculated for H-phase $MoSe_2$ and for the most stable nanowire. For the two-dimensional $MoSe_2$ a 4x4 supercell is used and for the one-dimensional ribbon a cell of 4 times the length of the unit cell.

It is good to mention that the above is based on a static calculation. However, according to Komsa et al.[11], this is in good agreement with the dynamically calculated displacement energy E_d. Therefore we here use $E^f_{vac,Se}$ to compare with the energy transferred by the electron beam E_e. E_e is much lower than the beam energy itself and can be calculated by:[38]

$$E_e = \frac{E_{beam}\left(E_{beam} + 2m_ec^2\right)}{E_{beam} + \left(1 + \frac{m_e}{M}\right)^2 \frac{Mc^2}{2}} \tag{3}$$

Here, M is the mass of the atom in the structure to which the energy is transferred. As can be seen in figure 16, the transferred energy is significantly lower than the beam energy. E_e has to be compared to $E^f_{vac,Se}$ to predict possible beam damage. However the two cannot be compared straight away, since E_e does not take into account how strong the atom is bound to the surrounding ones. Therefore, the needed electron voltage for beam damage should probably be significantly higher than the value found by a one to one comparison.

4 Results and Discussion

First, it is good to discuss pristine (H-phase) $MoSe_2$, to be better able to interpret changes upon heating. Figure 17 shows a model of H-phase $MoSe_2$ and high resolution TEM image.

This figure illustrates how this material looks at atomic scale. However when imaging in the electron microscope, one first has to find a suitable area in the flake of $MoSe_2$. Figure 18a shows a flake of $MoSe_2$. The shape and size is representative for the other flakes used in the experiments presented here. However, the thickness is not (figure 18b), which is atypical for the flakes observed in the electron microscope. There, for flakes of this size generally dozens of layers are stacked upon each other indicated by Moiré patterns visible. In this AFM image the

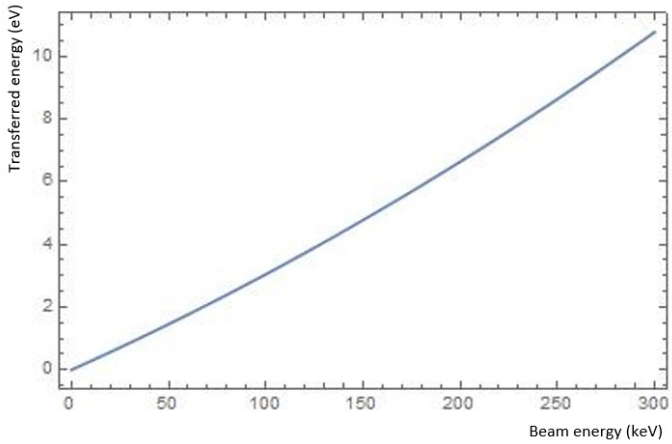

Figure 16: Tranferred energy to the structure as function of the beam energy (equation 3)

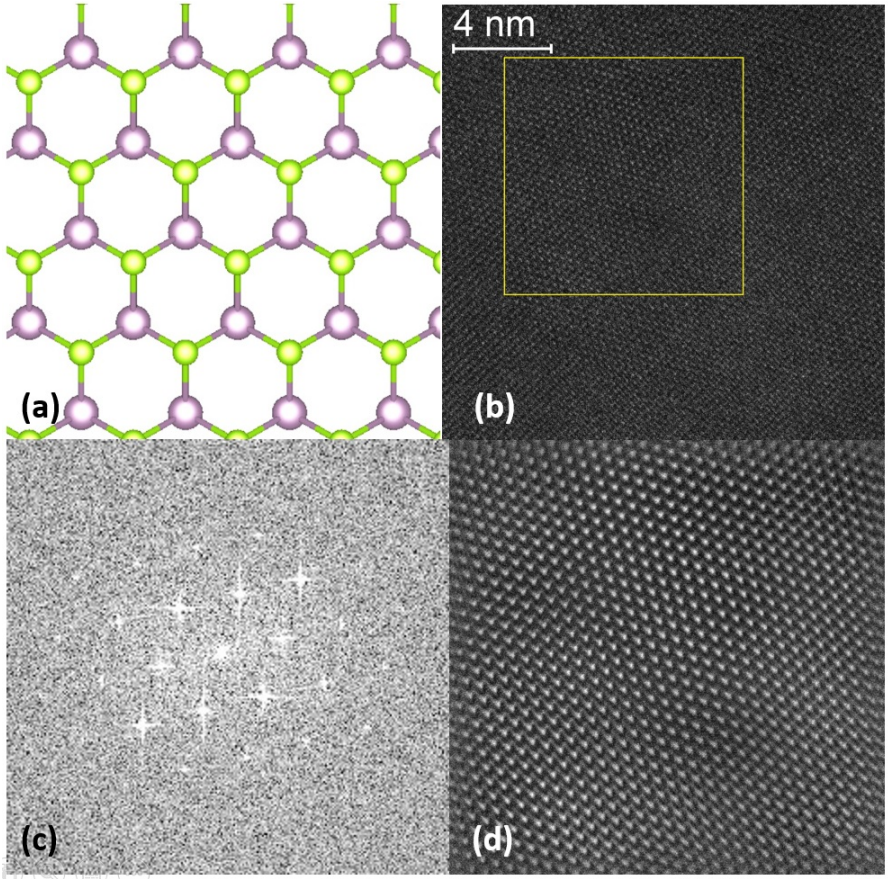

Figure 17: **(a)** Model of pristine H-phase $MoSe_2$. **(b)** High resolution TEM image of $MoSe_2$ at room temperature. **(c)** FFT of the area indicated in (b). The middle ring of dots indicate the family $[10\bar{1}0]$, the next ring the family $[11\bar{2}0]$. **(d)** Atomic lattice after Fourier masking the FFT.

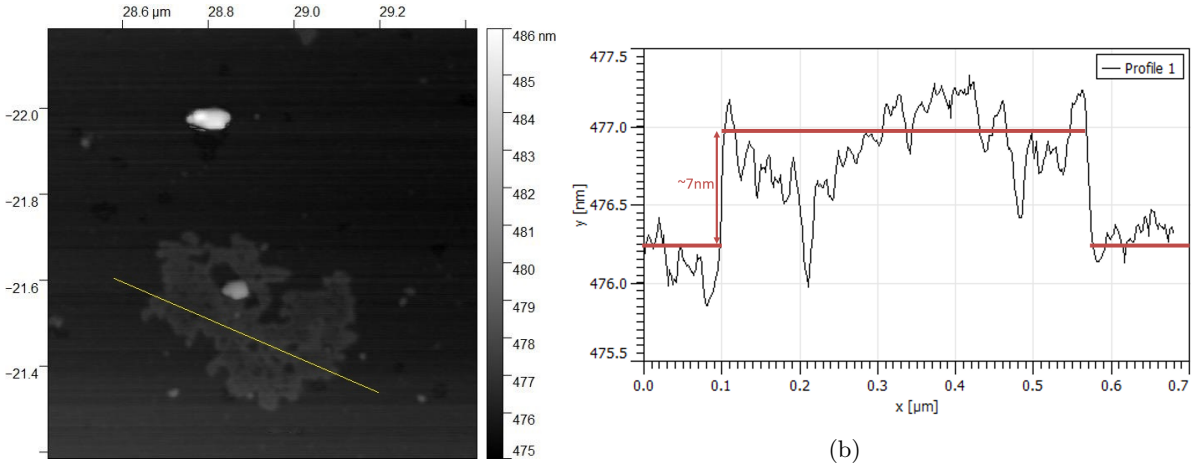

(a) (b)

Figure 18: **(a)** AFM image of a flake of $MoSe_2$. **(b)** Height profile along the line indicated in (a)

thickness of the flake is measured to be $\sim 7\,\text{Å}$, which is probably one layer $MoSe_2$. However, the height profile is not really flat, so for a more accurate measurement of the thickness a larger flake has to be measured in order to obtain a better mean of the height of a surface.

In figure 19 a STEM image of a typical flake of $MoSe_2$ is depicted. In this image it is clear that at the edges of multi-layered flakes, thinner areas are found. When doing (in-situ) experiments, generally the imaging is done at the edges of the flakes since there, there is the highest chance on having only a single orientation. Such a thin area which is a good spot for imaging is depicted in figure 20. Furthermore, EDX is used on this pristine flake (figure 19). Quantisation of this measurement resulted in Mo:Se ratio of 1:1.9 which is really close to the theoretically expected 1:2 ratio.

The electronic properties of H-phase $MoSe_2$ were calculated by DFT. The structure of the 1H-phase (fig. 4) was relaxed and also that of the 1T-phase to make a direct comparison. As expected, the H-phase has a slightly lower energy than the T-phase: respectively $-0.60\,\text{eV/atom}$ and $-0.37\,\text{eV/atom}$. Interesting to mention is the slight difference in cell size (not shape, both are strictly hexagonal) between 1H ($3.28\,\text{Å}$) and 1T ($3.23\,\text{Å}$). It is clear that there is a difference in lattice parameter between the phases. However, when doing experiments on this material, this is not a good way to differentiate between the two phases for two reasons: the difference is small and therefore hard to measure in TEM images and more importantly it is plausible that this distance is strongly dependent on temperature, whereas DFT calculations only handle structures at $0\,\text{K}$

For both the 1H- and 1T-phase the bandstructure and DOS (figures 21a and 21b) are determined. The electronic properties of the two differ: 1H is semiconducting (indirect band gap of $\sim 1.5\,\text{eV}$) and 1T is conducting (no band gap). From DOS-graphs which differentiate between the atom species (not shown here), it follows that the d-orbitals of the molybdenum atoms are the main contributors to the conduction in the 1T-phase.

Note that only monolayer phases are discussed here (therefore the '1' in 1T and 1H). Also bilayers and bulk phases have been briefly examined. However, those structures are not discussed here

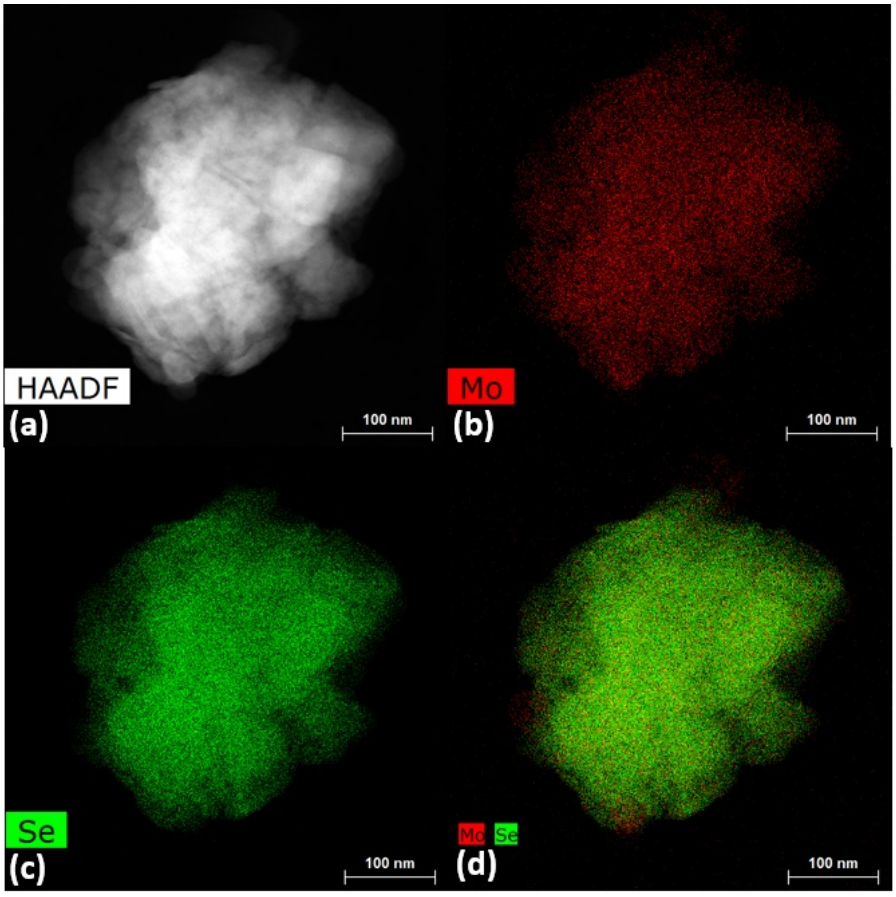

Figure 19: **(a)** STEM image of a typical $MoSe_2$ flake **(b)** EDX map showing Mo concentration **(c)** EDX map showing Se concentration **(d)** EDX map showing both Mo and Se

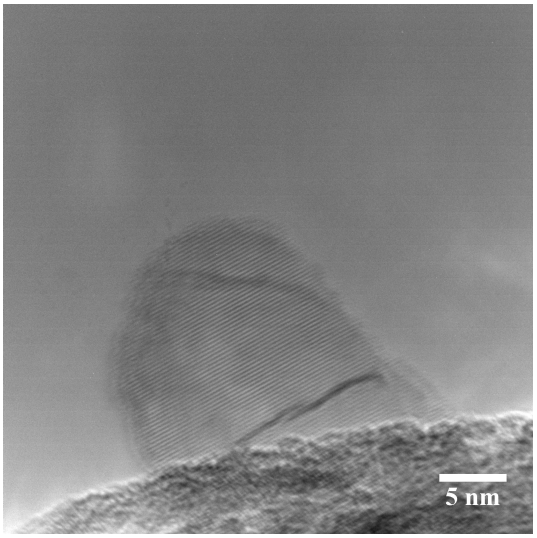

Figure 20: TEM images of the edge of a flake $MoSe_2$ with a thin part. Note the possibility for high resolution due to the disappeared Si_3N_4 background.

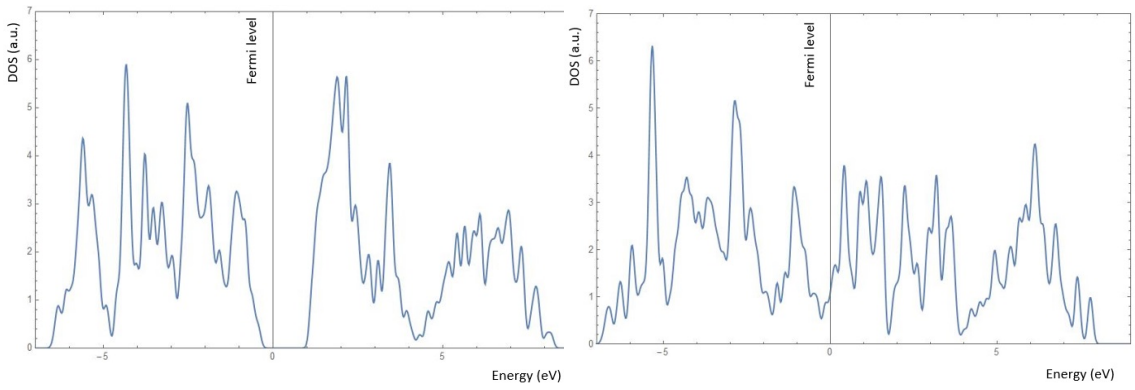

(a) Density of states of 1H-$MoSe_2$

(b) Density of states of 1T-$MoSe_2$

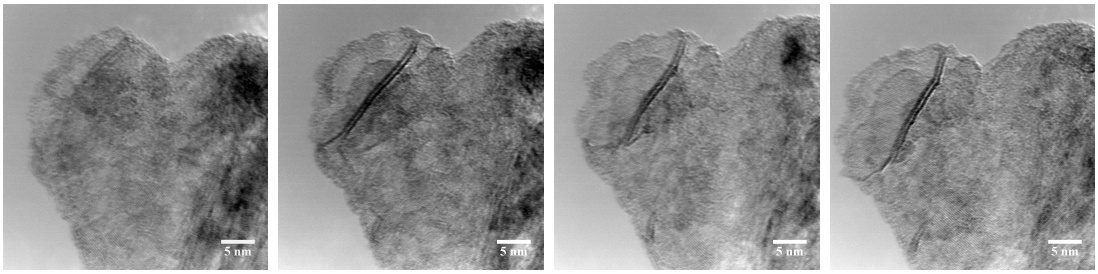

(a) (b) (c) (d)

Figure 22: Stills of TEM recording showing $MoSe_2$ with curling of the edge as an effect of the electron beam (imaged at room temperature). Between each subsequent image is about 1 minute of imaging.

since their properties resemble those of the monolayers, as expected the energy of these multilayer phases was found significantly lower than the monolayers due to the Van der Waals forces.

4.1 Edge effects and Etching

The edge of a flake is most susceptible for changes upon heating since here the atoms are most weakly bound. One of the first effects that was seen was an electron beam effect: the curling of edges (figure 22). This effect was also seen before heating the sample, so it purely is an electron beam effect.

This shows the destructive effect of the electron beam and emphasizes the importance of keeping electron doses low if imaging effects are desired to be minimized. However, what can be seen from these curling edges is the thickness of the layers. From another image with 13 layers visible on edge, the thickness of one layer was found to be 0.69 nm. Note that this measurement might not be very accurate since the angle of imaging is not known. AFM measurements presented as discussed in section 4 are probably more accurate.

When instead of deforming the sample, atoms are removed, it is called etching. For 1H-phase $MoSe_2$ the energy needed to remove a Se-atom is, calculated with equation 2: $E^f_{vac,Se} = 2.7\,\text{eV}$. Using equation 3, this results in a theoretical minimum for the threshold electron beam energy of around 89 keV. This thus is the theoretical minimum, in section 3.5.4 already was discussed that the true threshold probably is even higher due to the bonding energy in the material. Considering this, it makes sense that etching was found significantly more abundant at elevated temperatures. At high temperatures, a part of the energy to break the bond is already provided by the thermal energy. On top that, this minimum voltage only applies to a Se-atom in the middle of pristine $MoSe_2$, the atoms at an edge are more weakly bound in general. If one wants to prevent the removal of Se-atoms by the electron beam, only low-voltage TEM can be used. The used here used voltages of at minimum 200 keV do not count as low-voltage. How fast the etching process is at high temperature can be seen in figure 23.

The etching is not evenly favourable in all directions. The hexagonal nature of the material becomes visible here (figure 24), with almost all angles measured to be 120° and straight edges along the lines in the lattice. The resolution is just not good enough to conclude this with highest

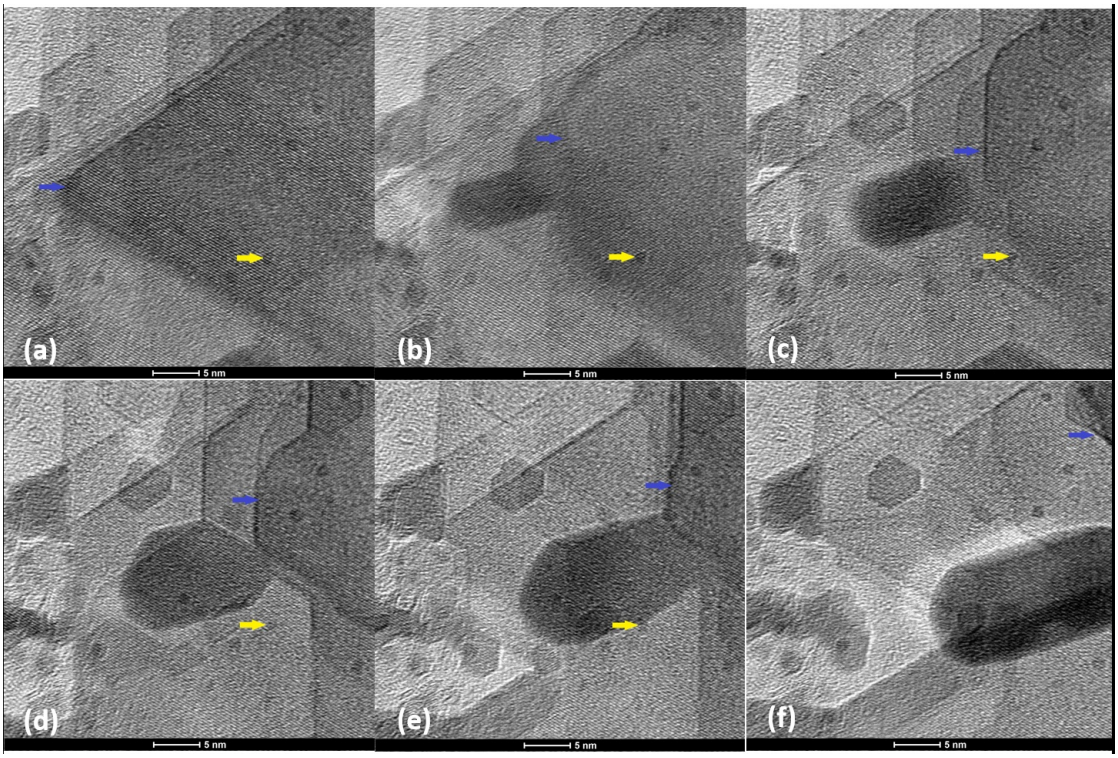

Figure 23: Stills of TEM recording showing edges of $MoSe_2$ etching at 1000 °C. Between two subsequent images is only around 10 seconds continuous imaging. Note the fast rate of etching indicated by the blue arrow. The yellow arrow is for reference indicating probably contamination.

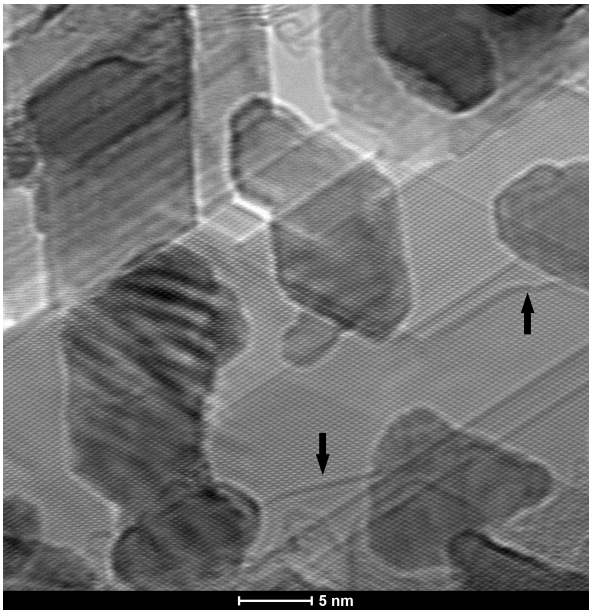

Figure 24: Result of etching off layers $MoSe_2$. Temperature: 750 °C

certainty, but it is assumed that these are all zigzag edges. The edges appearing dark at the TEM image might indicate an NW-terminating edge (as discussed by ref. [14]), however this cannot be stated with certainty since the darker appearence can also be an artefact of a subtle defocus. Two edges seen in figure 24 however do not comply with this (indicated with the black arrows). The edge indicated with the arrow at the right could possibly be an armchair edge since the angle with a zigzag edge is around 150°. However this is definitely not certain since the angle could not be measured properly due to the edge being quite short. Moreover, the edge indicated by the lower arrow is certainly not an armchair edge since the angle it makes with an zigzag edge is around 160°, so it is neither a zigzag nor armchair edge. It could be something in between, however it is not clear what kind of edge with this angle is stable. To investigate this better, these kind of edges should be more observed at first. On the other hand, it also is possible that it are not edges at all but nanowires, which can have all angles with respect to the lattice.

This severe etching effect at high temperatures show that exposing this material to high temperatures can make it thinner by etching away some layers. Investigating this thinning at elevated temperatures while not irradiated by the electron beam deserves some more attention, since here the effects by the beam can certainly not be ignored.

4.2 Nanowires

Combining high temperatures with beam irradiation not only results in proper etching along the lattice. When the temperature is high enough, spontaneous nanowires can form. It is not new to observe nanowires for this material, they were reported earlier by among others Liu et al.[17] Liu et al. produced this nanowires by making holes in the material with the electron beam; bringing two holes together resulted in a nanowire in between. In the current study the beam is not used to steer the nanowire formation, it is a spontaneous formation. Consequence is that the exact location where the ribbons form cannot yet be controlled. Figure 25 shows the formation of a network of nanowires from a first relatively pristine area $MoSe_2$.

The formation of the nanowires depicted in figures 25 was in the temperature range of 750 °C to 900 °C. However, it is plausible that not the rise in temperature but the long time of imaging (around 30 minutes for the series showed here) resulted in the observed phenomenon. In other words, at a constant temperature of 750 °C probably the same would have happened, but at a slower rate. The lowest temperature where these spontaneous nanowires were observed was 750 °C.

From the images it may be hard to distinguish between nanowires and edges as seen in figure 24. However this distinction is more easily made when looking at the videos from which the images are taken. Edges etch away due to the electron beam, the etching direction normally is perpendicular to the edge. Nanowires can be seen moving back and forth a bit without moving a significant distance. On top of that, the nanowires do not necessarily follow the lattice direction where edges do as discussed in section 4.1, at least for elevated temperatures. Furthermore please note the nanowire junction in the middle of figure 25. This resembles the nanowire junction made by Lin et al.[18].

Figure 26 shows a nanowire very clear without a background. The nanowire is not in focus completely, which makes it somewhat hard to measure or estimate the width of the nanowire. The nanowire being out of focus however makes it more clearly visible. A rough estimate of the

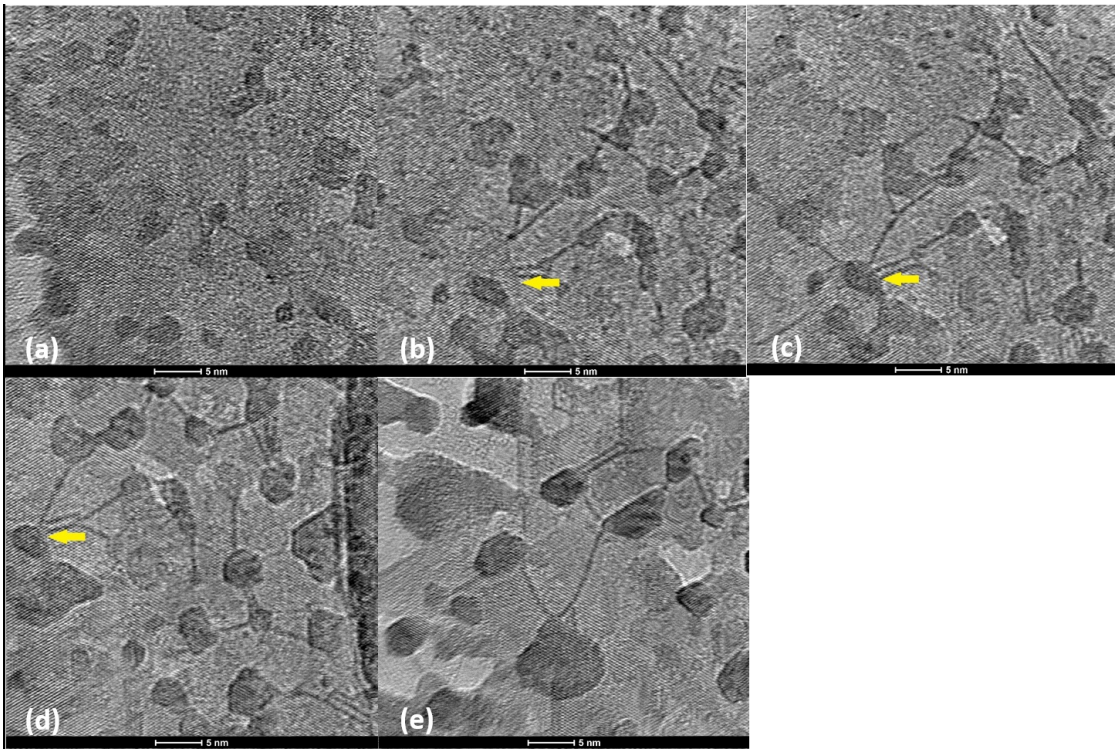

Figure 25: Consecutive TEM images of a nanowire network formation during continuous imaging. **(a)** 750 °C **(b)** 800 °C **(c)** 800 °C **(d)** 850 °C **(e)** 900 °C

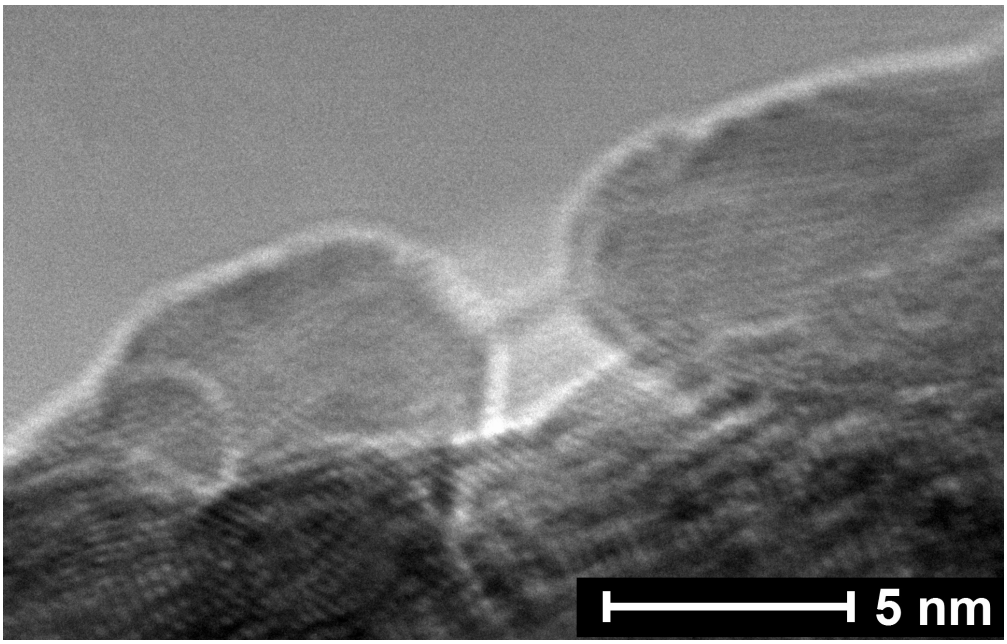

Figure 26: TEM image of nanowire seen without Si_3N_4 background. $T = 750\,°C$

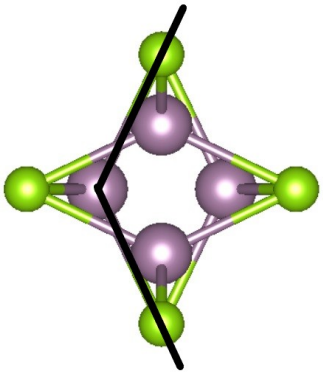

Figure 27: Lateral angle between the bonds, indicated for the Mo_4Se_4 nanowire.

width of the nanowire based on figure 26 is 5 Å, which is about three atomic layers.

From the five nanowires examined using DFT, the Mo_6Se_6 nanowire is energetically the most favourable with a formation energy of $-0.230\,\text{eV/atom}$. This is still a positive formation energy with respect to H-phase $MoSe_2$. Why the Mo_6Se_6 is more favourable than the other nanowires with comparable structure can esily be understood by looking at the atomic configuration of the nanowires (figures 11, 12, 13 and 14. We leave out the Mo_5Se_4 nanowire because of its different structure and significantly higher energy than the other four). Consider the angle between the bonds: the Se-Mo-Se angle in lateral direction (indicated for the Mo_4Se_4 nanowire in figure 27). This value differs much for the ribbons. When plotted, its deviation from 180 deg matches perfectly with the internal energy (figure 28). This observation can be explained by the steric hindrance between the Se-atoms. When the lateral angle is at its maximum, this hindrance is minimal and so is the energy. The longitudinal angle does not differ significantly between the nanowires. The height of the unit cell is also approximately the same.

The size of this Mo_6Se_6 (a width of 6 Å) nanowire matches perfectly with the nanowire seen in the heating experiment (an approximate width of 5 Å)

For the most stable nanowire, Mo_6Se_6, the DOS (figure 29) and magnetism were determined. Magnetic effects are not expected for the MoSe nanowire since the magnetic moments on the atoms are found equal to 0. As can be seen from the DOS, this nanowire does just as the 1T-phase not have a band gap, which makes the nanowire conducting. This is an interesting feature, because of the difference with the 1H-phase. If one is able to construct these nanowires in a controlled way, complex structures of semiconducting H-phase and conducting nanowires can be constructed.

Also for the Mo_6Se_6 nanowire, the threshold displacement energy is calculated with equation 2: $E^f_{vac,Se} = 2.4\,\text{eV}$. This slightly lower than the threshold displacement energy found for H-phase $MoSe_2$. It therefor is more favourable to remove a Se-atom from the nanowire than form the 1H-phase. However, the difference in vacancy formation energy is small and more importantly, Lin et al.[18] showed that the vacancy formation energy at the edge of the 1H-phase is even lower than that of the nanowire. This implies that vacancies from both the 1H-phase and the nanowire would travel to the edge, keeping both stable and self-healing. Noteworthy is that the threshold displacement energies for both the H-phase and the nanowire Lin et al. found are significantly higher than reported in the current study (about twice as high). Where this discrepancy comes

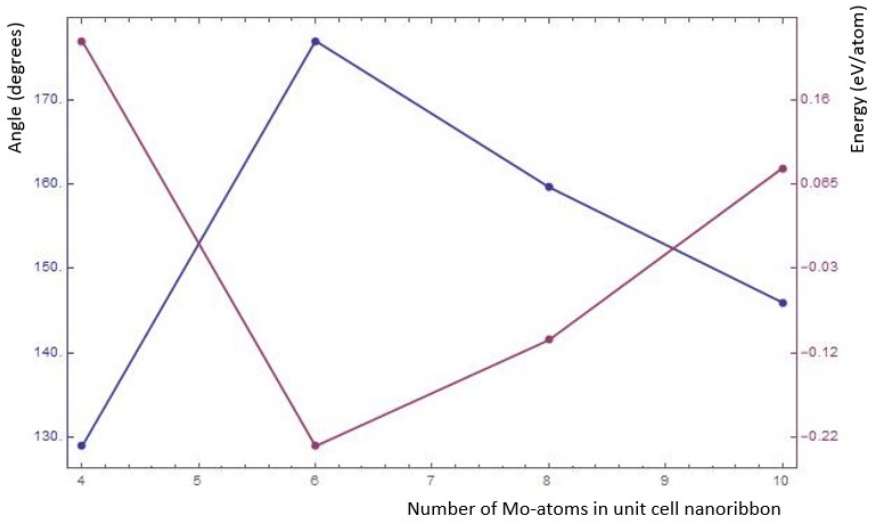

Figure 28: Lateral angle of the four different nanowires compared with the formation energy of these nanowires. The two are in perfect anticorrelation.

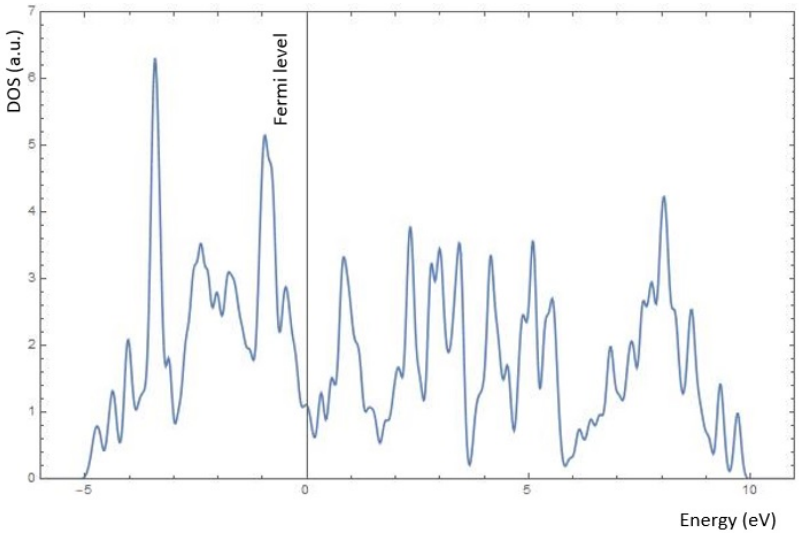

Figure 29: Density of states of Mo_6Se_6 nanowire

Table 2: Energies found for all investigated structures

Structure	Formation Energy (eV/atom)
Mo (BCC)	0 (by definition)
Se (hexagonal)	0 (by definition)
1H-$MoSe_2$	-0.599
1T-$MoSe_2$	-0.369
H-phase MoSe	-0.002
T-phase MoSe	-0.041
Flat hexagonal MoSe	1.578
Hexagonal MoSe	0.630
Square MoSe	1.460
Rectangular MoSe	1.309
Mo_4Se_4 Nanowire	0.226
Mo_6Se_6 Nanowire	-0.230
Mo_8Se_8 Nanowire	-0.110
$Mo_{10}Se_{10}$ Nanowire	0.083
Mo_5Se_4 Nanowire	0.690

from is not clear and should be looked into in more detail.

4.3 Other MoSe phases

Besides the nanowires also other kind of MoSe phases, listed in 3.5.2, were examined with DFT. The most important property of the phases is the formation energy, to determine which phases are energetically most favourable. All phases, inlcuding the nanowires already discussed in section 4.2, are shown in table 2.

Note that in table 2 also a new phase is added: flat, rectangular MoSe. During relaxation of the square phase it turned out that this rectangular phase, with unit cell length:width ratio 1:1.35, is energetically slightly more favourable. Though this is an interesting observation, in practice neither of the two phases will be oberved since both formation energies are high. The square phase could be prevented from relaxing to the rectangular shape by defining the initial unit cell perfectly square, upon which it remained in this meta-stable square configuration. However the rectangular MoSe clearly still is meta-stable (therefore the high energy) in z-direction. The structure is held flat artificially by defining the initial structure perfectly. This has an even larger effect on the energy, as is illustrated by the difference between hexagonal MoSe and perfectly flat hexagonal MoSe.

To quickly determine which phases might occur in practice, all energies are put together in a concave-hull plot (figure 30). It is clear directly that the 1H-phase is most stable and that none of the MoSe phases has an energy sufficiently low to be stable. However, as mentioned before, DFT calculations do not tell anything about kinetics. Since the energy for some phases to form is only 0.2 eV/atom or 0.3 eV/atom, it is reasonable that these relatively low-energy phases (e.g. the Mo_6Se_6 nanowire or the MoSe T-bulk phase) might be observed in practice, as was the case in this study. Especially when irradiating with an electron beam in an electron microscope, there is a change to form these phases since energy is provided by the electron beam. A sidenote that

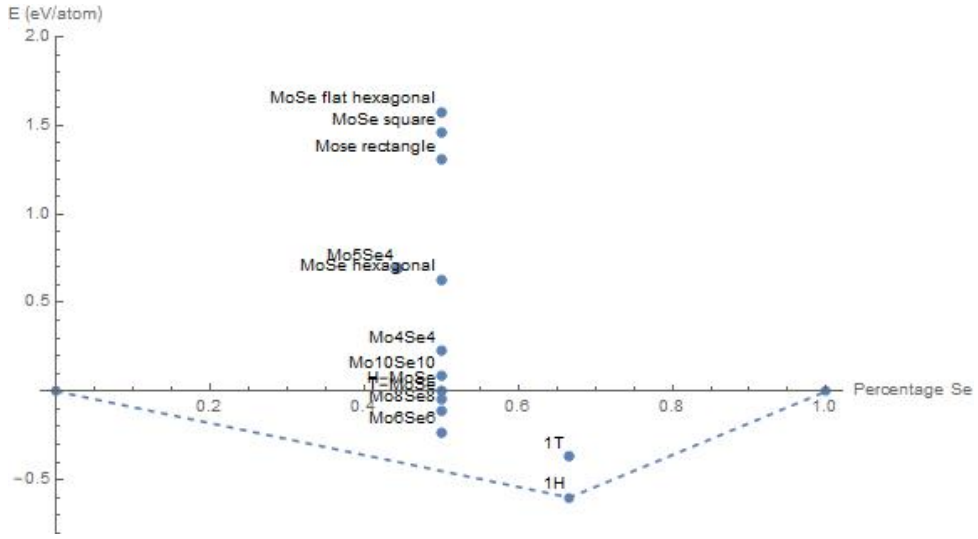

Figure 30: Concave-hull plot of all structures examined. The $MoSe_2$ H-phase is the most stable.

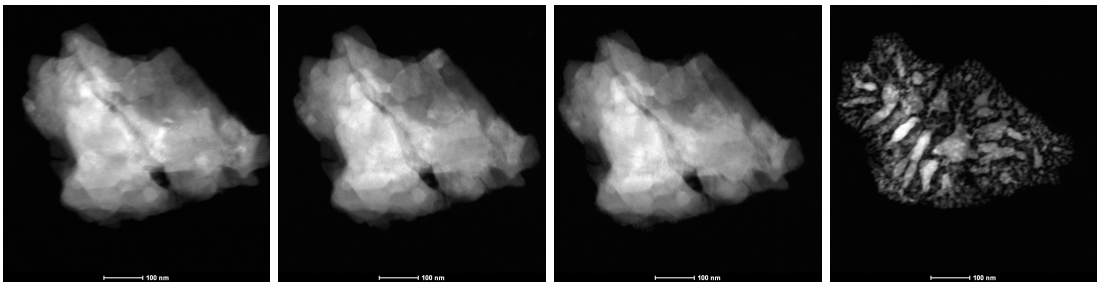

(a) $T = 20\,^{\circ}\mathrm{C}$ (b) $T = 800\,^{\circ}\mathrm{C}$ (c) $T = 900\,^{\circ}\mathrm{C}$ (d) $T = 950\,^{\circ}\mathrm{C}$

Figure 31: Consecutive STEM images of continuous in-situ heating of $MoSe_2$ up to $950\,^{\circ}\mathrm{C}$

has to be made is that the pristine H-phase $MoSe_2$ here is monolayer, whereas in experiment mostly it is found in multilayer having a lower energy. Then the energy difference with the other phases is somewhat higher.

In the in-situ TEM experiments in this study, no indications were found that other phases than the H-phase and the nanowire phase were present. This is not surprising since the H-phase of has the lowest energy and the Mo_6Se_6 nanowire has the lowest energy for a reduced selenium concentration.

4.4 Energy-dispersive X-ray crystallography

As mentioned in section 3.3, EDX is important for investigating the ratio between molybdenum and selenium. Heating has an enormous effect on a flake of $MoSe_2$ (figure 31).

To interpret the STEM images in figure 31 in an appropriate way, one must know that the

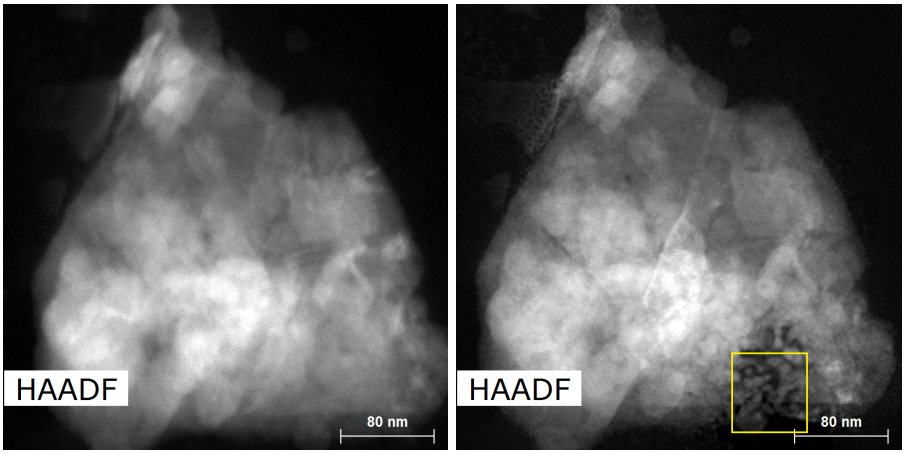

(a) $T = 20\,^{\circ}\mathrm{C}$ (b) $T = 800\,^{\circ}\mathrm{C}$

Figure 32: STEM images of the effect of in-situ heating up to 800 °C. Only the right-bottom part of the flake has been irradiated by the electron beam. The atomic ratios have been determined by EDX **(a)** Mo:Se ratio 1:1.85 **(b)** Mo:Se ratio 1:1.59 (whole frame). Mo:Se ratio 1:0.47 (yellow square)

time between images 31a and 31b is a couple of hours, the time between images 31b and 31c is only a few minutes and the time between images 31c and 31d is about 30 minutes imaging this flake at 900 °C. Other flakes in this same experiment looked the same after heating to 950 °C, which means that this is not (only) an electron beam effect. In a later experiment, the a similar evolution was observed (figures 32). Up to 800 °C the Mo:Se ratio only deviates significantly from the theoretical 1:2 for pristine $MoSe_2$ when irradiated by the electron beam. In a following heating experiment, the same sample of figure 32 was heated further to above 900 °C and now the whole flake had become poorer in selenium.

It is good to look again to figure 25. Because these images were taken at 750 °C, the Mo:Se ratio would not change by heating only. By making this images, the area was irradiated intensively. Some formed 'islands' are therefore suspected to be metallic molybdenum instead of a compound consisting of both molybdenum and selenium. Especially the dark appearing 'islands' are suspected to be molybedum. In one of them lattice fringes were visible (figure 33), which are closer together (2.7 Å) than what would be expected for $MoSe_2$ (3.3 Å). A distance of 2.7 Å corresponds to what could be expected for BCC elemental molybdenum. The TEM image in figure 34 gives some more proof, it depicts an area with some nanowires. From the EDX measurement, it follows that there indeed are parts with only molybdenum.

5 Conclusions and Outlook

Heating experiments done here show that there are some interesting phenomena happening at elevated temperatures before $MoSe_2$ decomposes completely where decomposing in the electron microscope is obeserved as elemental molybdenum remaining and the selenium sublimating into the vacuum. Until a temperature of around 850 °C the Mo:Se ratio can only be changed signifi-

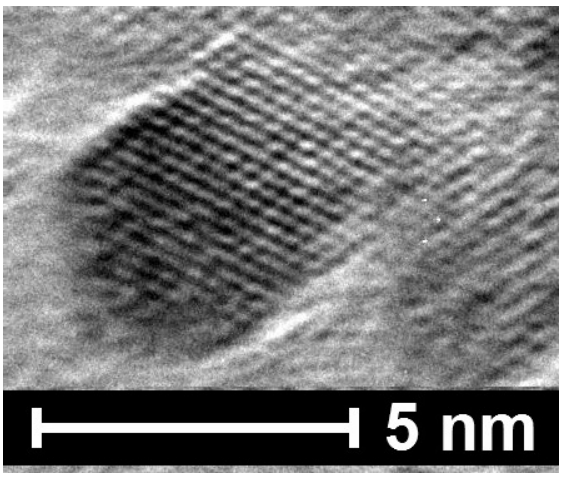

Figure 33: TEM image of molybedum 'islands' as part of a nanowire network at 900 °C

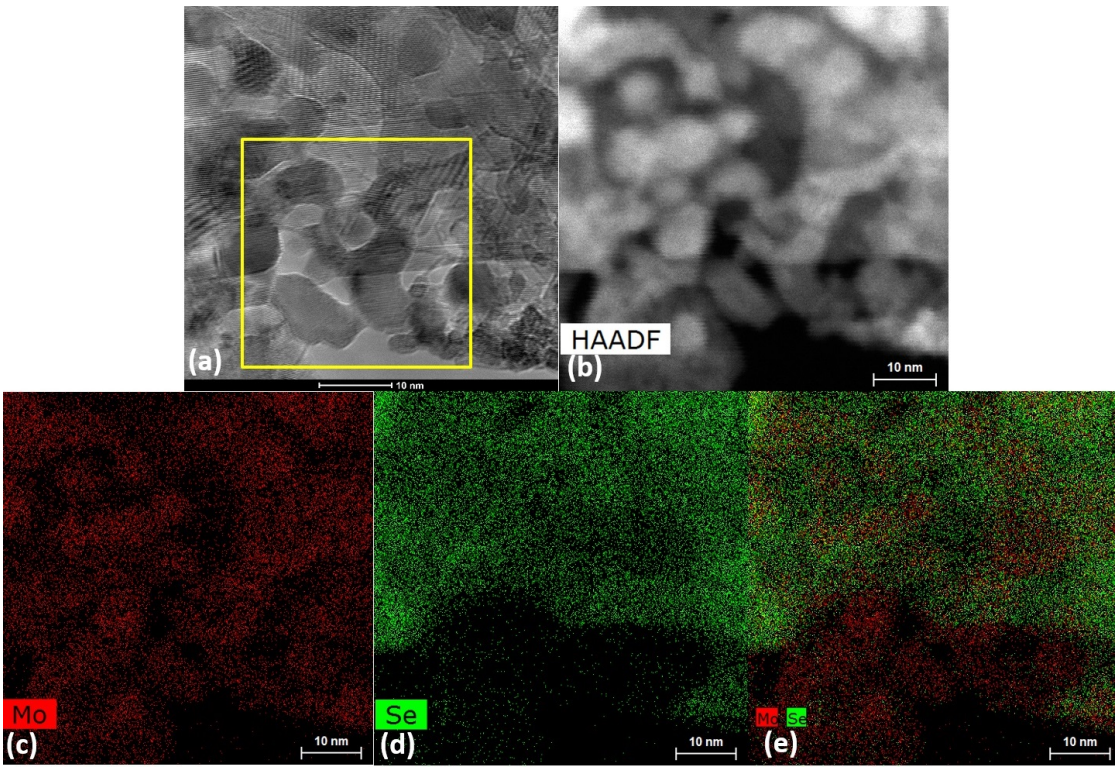

Figure 34: Images of the right-bottom part of the flake in figure 32 $T = 800\,°C$ **(a)** TEM image **(b)** STEM image of approximately the area indicated with the squares in figure (a) and 31b The EDX maps in (c)-(e) show this same area. **(c)** EDX map showing Mo concentration **(d)** EDX map showing Se concentration **(e)** EDX map showing both Mo and Se

cantly by electron beam irradiation and not by heating only, above this temperature sublimation of the selenium is spontaneous. However when combined with the electron beam, some interesting structures can be created, like 'islands' of $MoSe_2$ or elemental molybdenum with MoSe-nanowires in between. Especially this last observation deserves some follow-up research since it could be interesting for electronic applications. In this study, we have not been able to control the location of the nanowire formation. Whenever the temperature is not too high, e.g. around 750 °C and the beam irradiation not too strong, there are definitely opportunities to focus the electron beam on certain areas in order to control the formation process. Furthermore additional experiments with slightly better resolution are required to distinguish between the H-phase and the T-phase. One of the goals of this study was to determine whether the T-phase would be seen at elevated temperatures. However even after Fourier-filtering the images with atomic resolution, the distinction between the phases could not be made unambiguously. The same holds for the behaviour of defects when exposed to high temperatures. Resolution did not allow for tracking any defects.

DFT supports the possible applications. In line with literature, the H-phase is found to be semiconducting and the T-phase is metallic. The nanowires found in experiment are confirmed to be Mo_6Se_6 nanowires which are also metallic. Although it has a higher threshold displacement energy than pristine $MoSe_2$ (respectively 2.4 eV and 2.7 eV), the nanowire is stable since the threshold displacement energy at the edges can be expected to be lower.

Besides nanowires, also other phases have been examined. However most have an unexpectedly high formation energy, from which the conclusion is drawn that those will not be found in experiment. Based on the phases examined, the only three phases that are likely to be found are the pristine H-phase, the slightly higher in energy T-phase and the Mo_6Se_6 nanowire. As discussed, all three have been observed, in this study or in literature.

A final conclusion that can be drawn from this study is the thinning of the material due to the sublimation discussed above alongside the straightening of the edges of the layers. Although the straightening of edges has only been observed under irradiation with the electron beam, it is reasonable to suspect this also to happen without the electron beam. Additions experiments are needed to confirm this. In addition, DFT calculations on the edges have not been done in this study, but would be helpful for understanding these edge effects.

References

[1] Chen Luo, Chaolun Wang, Xing Wu, Jian Zhang, and Junhao Chu. In situ transmission electron microscopy characterization and manipulation of two-dimensional layered materials beyond graphene. *Small*, 2017.

[2] Q.H. Wang, K Kalantar-Zadeh, A Kis, J.N. Coleman, and M.S. Strano. Electronics and optoelectronics of two-dimensional transition metal dichalcogenides. *Nature Nanotechnology*, 7:699–712, 2012.

[3] Ali Jawaid, Dhriti Nepal, Kyoungweon Park, Michael Jespersen, Anthony Qualley, Peter Mirau, Lawrence F. Drummy, and Richard A. Vaia. Mechanism for liquid phase exfoliation of mos2. *Chemistry of Materials*, 28(1):337–348, 2016.

[4] Per Joensen, R.F. Frindt, and S. Roy Morrison. Single-layer mos_2. *Materials Research*

Bulletin, 21(4):457–461, 1986.

[5] Xingli Wang, Yongji Gong, Gang Shi, Wai Leong Chow, Kunttal Keyshar, Gonglan Ye, Robert Vajtai, Jun Lou, Zheng Liu, Emilie Ringe, Beng Kang Tay, and Pulickel M. Ajayan. Chemical vapor deposition growth of crystalline monolayer mose2. *ACS Nano*, 8(5):5125–5131, 2014. PMID: 24680389.

[6] Yung-Chang Lin, Dumitru O. Dumcenco, Ying-Sheng Huang, and Kazu Suenaga. Atomic mechanism of the semiconducting-to-metallic phase transition in single-layered mos2. *Nature Nanotechnology*, 9:391 EP –, Apr 2014. Article.

[7] Xiaolong Zou, Yuanyue Liu, and Boris I. Yakobson. Predicting dislocations and grain boundaries in two-dimensional metal-disulfides from the first principles. *Nano Letters*, 13(1):253–258, 2013. PMID: 23227928.

[8] R. A. Gordon, D. Yang, E. D. Crozier, D. T. Jiang, and R. F. Frindt. Structures of exfoliated single layers of ws_2, mos_2, and $mose_2$ in aqueous suspension. *Phys. Rev. B*, 65:125407, Mar 2002.

[9] Xin Lu, M. Iqbal Bakti Utama, Junhao Lin, Xue Gong, Jun Zhang, Yanyuan Zhao, Sokrates T. Pantelides, Jingxian Wang, Zhili Dong, Zheng Liu, Wu Zhou, and Qihua Xiong. Large-area synthesis of monolayer and few-layer mose2 films on sio2 substrates. *Nano Letters*, 14(5):2419–2425, 2014. PMID: 24678857.

[10] Wu Zhou, Xiaolong Zou, Sina Najmaei, Zheng Liu, Yumeng Shi, Jing Kong, Jun Lou, Pulickel M. Ajayan, Boris I. Yakobson, and Juan-Carlos Idrobo. Intrinsic structural defects in monolayer molybdenum disulfide. *Nano Letters*, 13(6):2615–2622, Jun 2013.

[11] Hannu-Pekka Komsa, Jani Kotakoski, Simon Kurasch, Ossi Lehtinen, Ute Kaiser, and Arkady V. Krasheninnikov. Two-dimensional transition metal dichalcogenides under electron irradiation: Defect production and doping. *Phys. Rev. Lett.*, 109:035503, Jul 2012.

[12] Yuanyue Liu, Xiaolong Zou, and Boris I. Yakobson. Dislocations and grain boundaries in two-dimensional boron nitride. *ACS Nano*, 6(8):7053–7058, 2012. PMID: 22780217.

[13] Ossi Lehtinen, Hannu-Pekka Komsa, Artem Pulkin, Michael Brian Whitwick, Ming-Wei Chen, Tibor Lehnert, Michael J. Mohn, Oleg V. Yazyev, Andras Kis, Ute Kaiser, and Arkady V. Krasheninnikov. Atomic scale microstructure and properties of se-deficient two-dimensional mose2. *ACS Nano*, 9(3):3274–3283, 2015. PMID: 25748134.

[14] Xiahan Sang, Xufan Li, Wen Zhao, Jichen Dong, Christopher M. Rouleau, David B. Geohegan, Feng Ding, Kai Xiao, and Raymond R. Unocic. In situ edge engineering in two-dimensional transition metal dichalcogenides. *Nature Communications*, 9(1):2051, 2018.

[15] Florian Banhart. *In-Situ Electron Microscopy at High Resolution.*

[16] David B. Williams and C. Barry Carter. *Transmission Electron Microscopy A textbook for Materials Science.*

[17] Xiaofei Liu, Tao Xu, Xing Wu, Zhuhua Zhang, Jin Yu, Hao Qiu, Jin-Hua Hong, Chuan-Hong Jin, Ji-Xue Li, Xin-Ran Wang, Li-Tao Sun, and Wanlin Guo. Top-down fabrication of sub-nanometre semiconducting nanoribbons derived from molybdenum disulfide sheets. *Nature Communications*, 4:1776 EP –, Apr 2013. Article.

[18] Junhao Lin, Ovidiu Cretu, Wu Zhou, Kazu Suenaga, Dhiraj Prasai, Kirill I. Bolotin, Nguyen Thanh Cuong, Minoru Otani, Susumu Okada, Andrew R. Lupini, Juan-Carlos Idrobo, Dave Caudel, Arnold Burger, Nirmal J. Ghimire, Jiaqiang Yan, David G. Mandrus, Stephen J. Pennycook, and Sokrates T. Pantelides. Flexible metallic nanowires with self-adaptive contacts to semiconducting transition-metal dichalcogenide monolayers. *Nature Nanotechnology*, 9:436–442, Apr 2014.

[19] J.M. Tarascon, F.J. DiSalvo, C.H. Chen, P.J. Carroll, M. Walsh, and L. Rupp. First example of monodispersed (mo3se3) clusters. *J. Solid State Chem.*, 58:290–300, 1985.

[20] Latha Venkataraman and Charles M. Lieber. Molybdenum selenide molecular wires as one-dimensional conductors. *Phys. Rev. Lett.*, 83:5334–5337, Dec 1999.

[21] Nicole Zink, Helen Annal Therese, Julien Pansiot, Aswani Yella, Florian Banhart, and Wolfgang Tremel. In situ heating tem study of onion-like ws2 and mos2 nanostructures obtained via mocvd. *Chemistry of Materials*, 20(1):65–71, 2008.

[22] William A Brainard. The thermal stability and friction of the disulfides, diselenides, and ditellurides of molybdenum and tungsten in vacuum (10^{-9} to 10^{-6} torr). *NASA Technical Note*, 1969.

[23] P. Hohenberg and W. Kohn. Inhomogeneous electron gas. *Phys. Rev.*, 136:B864–B871, Nov 1964.

[24] H. van Gog. Thermische stabiliteit van tweedimensionale mangaanoxides. *Nederlands Tijdschrift voor Natuurkunde*, pages 18–22, April 2019.

[25] Rik Koster. *How Surfaces Determine the Properties of Nanomaterials. A Density Functional Theory Study.*

[26] G. Kresse and J. Hafner. Ab initio molecular dynanics for liquid metals. 47:558, 1993.

[27] G. Kresse and J. Hafner. Ab initio molecular-dynanics simulation of the liquid-metal-amorphous-semiconductor transition in germanium.

[28] G. Kresse and J. Furthmüller. Efficiency of ab initio total energy calculations for metals and semiconductors using a plane-wave basis set.

[29] G. Kresse and J. Furthmüller. Efficient iterative schemes for ab initio total-energy calculations using a plane-wave basis set.

[30] P.E. Blöchl. Projector augmented-wave method. *Phys. Rev. B*, 50:17953, 1994.

[31] G. Kresse and J. Joubert. Fron ultrasoft pseudopotentials to the projector augmented wave method. *Phys. Rev. B*, 59:1758, 1999.

[32] P. Perdew, K. Burke, and M. Ernzerhof. Generalized gradient approximatuin made simple. *Phys. Rev. Lett.*, 77:3865, 1996.

[33] S. Grimme, J. Antony, S. Ehrlich, and S. Krieg. *J. Chem. Phys.*, 132:154104, 2010.

[34] S. Grimme, S. Ehrlich, and L. Goerigk. *J. Comp. Chem.*, 32:1456, 2011.

[35] K. Momma and F. Izumi. Vesta 3 for three-dimensional visualization of crystal, vulumetric

and morphology data. *J. Appl. Crystallogr.*, 44:1272–1276, 2011.

[36] Alina Shafqat, Tahir Iqbal, and Abdul Majid. A dft study of intrinsic point defects in monolayer mose 2. *AIP Advances*, 7:105306, 10 2017.

[37] P. Murugan, Vijay Kumar, Yoshiyuki Kawazoe, and Norio Ota. Assembling nanowires from mos clusters and effects of iodine doping on electronic structure. *Nano Letters*, 7(8):2214–2219, 2007. PMID: 17625902.

[38] Hengfei Gu, Geping Li, Chengze Liu, Fusen Yuan, Fuzhou Han, Lifeng Zhang, and Songquan Wu. Considerable knock-on displacement of metal atoms under a low energy electron beam. *Sci Rep*, 7(1):184–184, Mar 2017. 28298631[pmid].